Influence of the Spinning Conditions on the Structure and Properties of Polyamide 12/Carbon Nanotube Composite Fibers

Carine Perrot,[1,2] Patrick M. Piccione,[2] Cécile Zakri,[1] Patrice Gaillard,[2] Philippe Poulin[1]

[1]*Centre de Recherche Paul Pascal, Centre National de la Recherche Scientifique, Université de Bordeaux, Avenue Schweitzer, Pessac 33600, France*
[2]*Groupement de Recherches de Lacq, Arkema, BP 34, Lacq 64170, France*

Received 25 February 2009; accepted 3 June 2009
DOI 10.1002/app.30875
Published online 12 August 2009 in Wiley InterScience (www.interscience.wiley.com).

ABSTRACT: The inclusion of nanoparticles in polymer fibers is potentially useful for improving or bringing new properties such as mechanical strength, electrical conductivity, piezoresistivity, and flame retardancy. In this study, composite fibers made of polyamide 12 and multiwall carbon nanotubes were investigated. The fibers were spun via a melt-spinning process and stretched at different draw ratios. The influence of several spinning factors, including spinning speed, extrusion rate, and draw ratio were investigated and correlated to the structure and properties of the fibers. X-ray diffraction analyses and mechanical tests indicated that the spinning speed barely affected the structure and mechanical properties of the fibers under tension. The spinning speed, however, is critical for future industrial applications because it determines the possible production rates. By contrast, drawing during spinning or after spinning strongly affected the polymer chain alignment and fiber mechanical properties. © 2009 Wiley Periodicals, Inc. J Appl Polym Sci 114: 3515–3523, 2009

Key words: extrusion; fibers; nanocomposites; polyamides

INTRODUCTION

Carbon nanotubes (CNTs) exhibit tensile modulus and strength values on the order of 1 TPa[1,2] and 60 GPa,[3,4] respectively. They exhibit a large aspect ratio and high electrical[5] and thermal conductivities.[6] The combination of these distinctive features make them promising for blending with polymers to obtain low-density nanocomposites with new or improved mechanical, electrical, and thermal properties.[7–15]

Although individual nanotubes exhibit exceptional properties on the nanometric scale, manifesting these properties on a macroscopic scale remains challenging. Good control of the dispersion is required in addition to a high degree of alignment of individual nanotubes within the polymer matrix. Fiber spinning has been developed over several decades to produce high-performance polymer fibers through polymer chain alignment.[16] In the same spirit, spinning approaches have been currently explored for CNTs.[17] Innovative processes, such as direct spinning[18–23] or coagulation spinning[24–28] for high CNT contents up to pure CNT fibers, have been reported. Other approaches have been based on more traditional processes, such as the melt spinning of CNT–polymer composites prepared by typical thermoplastic compounding in the melt state[29–35] or by the use of a solvent and a liquid suspension of nanotubes.[36–41] Mainly because of the viscosity increase, only low CNT fractions can be incorporated in thermoplastic polymers by melt-spinning approaches. Nevertheless, melt spinning remains the most common method for large-scale fiber manufacture because this process allows high-speed production rates and low production costs.

Haggenmueller et al.[37] reported an increase in the elastic modulus and yield stress of single-wall nanotube (SWNT)/poly(methyl methacrylate) (PMMA) composite fibers with nanotube loading and draw ratio. They reported a significant alignment for the higher draw ratios, with an orientation distribution as low as 4° for a draw ratio of 300. Fischer et al.[31] studied the influence of the draw ratio on the alignment of nanotubes in a polycarbonate–CNT system by polarized Raman spectroscopy and transmission electron microscopy. The mechanical properties of these fibers were investigated by Pötschke et al.[42] They reported an increase in the Young's modulus with draw ratio. This was assigned to the higher orientation of the polymer chains and the nanotubes at

Correspondence to: P. Poulin (poulin@crpp-bordeaux.cnrs.fr).

Contract grant sponsors: Arkema, Nanocomposite Materials Project of the Aerospace Valley and Aquitaine Region (NACOMAT project).

great take-up velocities. It has also been shown that drawing at low temperatures[43,44] leads to an improvement in the breaking strain together with a lower failure strength and little variation in the Young's modulus.

The objective of this study was to systematically investigate the influence of different spinning conditions, that is, screw rotation speed, spinning speed, and postdrawing ratio, on the morphology and mechanical properties of polyamide 12 (PA12)/multiwall nanotube (MWNT) composite fibers. Linear aliphatic polyamides are widely used as engineering materials and fibers. They exhibit relatively high modulus, toughness, and strength values, together with low creep and a satisfactory temperature resistance. Within the polyamide family, polyamide 6 and polyamide 6,6 are by far the fibers with the largest tonnage manufactured for textile and engineering applications. PA12 fibers only represent a small fraction of the polyamide fiber market, but they exhibit an excellent strength/toughness balance. Sandler et al.[45] studied PA12–nanotube composite fibers. They compared the potential of various multiwall CNTs and nanofibers as mechanical reinforcements in such fibers. The best results, both in terms of dispersion and mechanical property improvements, were obtained with vapor-grown carbon nanofibers and chemical vapor deposition grown multiwall CNTs. Although the effect of alignment was not systematically studied, the authors reported that a sample drawn to 100% did not exhibit significant improvements in CNT alignment compared to undrawn fibers.

In this study, PA12–MWNT fibers were produced by systematic variation of the processing parameters. The fiber morphology was studied by scanning electron microscopy (SEM), and the linear density was measured. Polymer chains and nanotube orientations were characterized by X-ray diffraction. Last, the influence of nanotube alignment on the mechanical properties of the nanocomposite fibers was investigated.

Postspinning treatments had a greater impact than the spinning conditions on the structure of the fibers. Postspinning treatments indeed allowed significant improvements in CNT alignment. These structural modifications were correlated to the variations in the mechanical properties.

EXPERIMENTAL

Materials and melt spinning

AMNO TLD-grade PA12 (hereafter, just PA12) and C100-grade Graphistrength multiwall CNTs produced by a catalyzed chemical vapor deposition process were used throughout the study. The average external diameter of the tubes varied typically from 10 to 15 nm. Both the polymers and MWNTs were provided by Arkema (France). The nanotubes were used without purification. The PA12 composites with nanotube concentrations of 3 and 7 wt % (PA12–3NT and PA12–7NT, respectively) were produced by Arkema by the mixture of materials on an adapted melt-compounding machine and were provided in pellet form. The dispersions exhibited a homogeneous texture when thin sections were observed with an optical microscope. This reflected the absence of aggregates larger than a micrometer typically. Single-filament melt spinning was performed with the experimental spinning equipment shown in Figure 1. Before processing, the nanotube–PA12 blends were dried overnight at 80°C *in vacuo.* The dried composites were placed in an extruder and heated between 200 and 220°C. The molten polymer was forced through a spinneret with a constant-speed drive, which could be adjusted to modify the mass flow rate of the polymer. The spinneret was a cylindrical capillary, which was 1 mm in diameter. The fiber was wound up around the rollers of the first drawing bench. Its linear speed could be increased up to 27.5 m/min. A drawing step was then carried out. It consisted of the stretching of the fibers to increase the nanotube orientation. In this study, the drawing treatment was performed during spinning via a second drawing bench. The speed of the rolls of this second bench was higher than the speed of the first bench and could go up to 175.6 m/min. An oven, through which the fiber circulated, was placed between the first and the second drawing benches (Fig. 1). The oven was 1.50 m long, and its temperature was fixed at 120°C throughout the study. The drawing ratio was defined as the ratio of the second drawing bench linear speed to the linear speed of the first one. The typical diameter of the

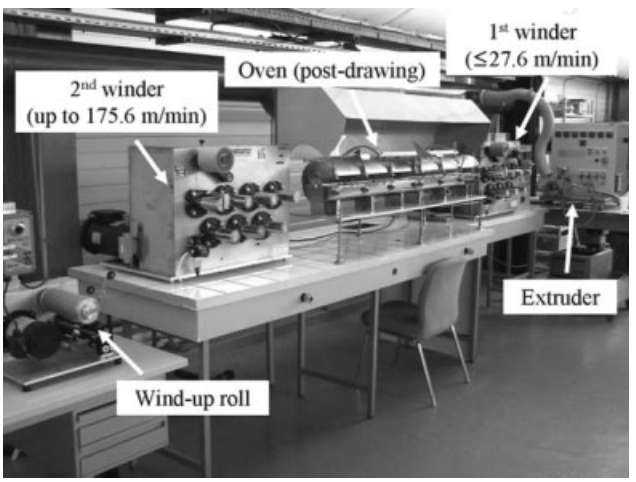

Figure 1 Experimental single-filament melt-spinning line used to make composite MWNT–PA12 fibers.

presently investigated fibers was in the range 70–130 μm, depending on the drawing ratio. The fibers broke when the spinning speed was too high. This limited the maximum achievable drawing ratio. The addition of CNTs was found to reduce this maximum during spinning. Such a behavior was already observed for polypropylene fibers.[38] No CNT-containing fiber could be directly drawn on this spinning line with a draw ratio greater than 3. A draw ratio of 5 was reached for the pure PA12 fibers. Hot drawing after spinning, however, allowed drawing ratios as high as 7 to be achieved for both kinds of fibers without breaking. For this procedure, the fiber samples were first collected on a roller. A piece of fiber was then simply cut and stretched with a tensile device placed in an oven. This setup allowed a drawing speed slower than that achieved with the rollers of the spinning line. In this case, the draw ratio was directly deduced from the fiber strain. The diameter of the fibers obtained by this procedure could be lower than 60 μm.

Morphological analyses

The structure of the PA12–MWNT composite fibers was investigated both qualitatively and quantitatively. The dispersion and orientation of the nanotubes were estimated by SEM, and the orientation of the CNTs was determined by X-ray diffraction.

SEM

A JEOL JSM-6700F field emission scanning electron microscope operating at 3 kV was used to observe the dispersion of CNTs in the polymer matrix. The samples were cryofractured in nitrogen perpendicular to the fiber axis to examine the fiber cross sections. Some samples were split parallel to the fiber axis during fracture to visualize the nanotube orientation along the fiber axis. Both drawn and undrawn composite fibers were imaged.

It is well established that the nanotube aspect ratio strongly influences the reinforcement capabilities.[46–48] SEM was, therefore, used to estimate the nanotubes length before and after compounding with the polymer. The composite was dissolved in a phenol/trichlorobenzene mixture. A drop of the dispersion thus obtained was deposited on an SEM mount and dried. It was then gently washed several times with pure solvent to remove the polymer. Finally, the dried deposit was imaged to compare MWNTs before and after melt compounding.

X-ray diffraction

The orientation of the CNTs within the fibers was characterized by X-ray diffraction with a Rigaku Nanoviewer apparatus equipped with a rotating Cu anode generator operating at 40 kV and 20 mA. The two-dimensional scattering pattern was collected with a Mercury charged coupling device camera. The sample–detector distance was fixed at 77 mm (wave vector ≤ 2.89 Å^{-1}). An air scattering pattern with no sample was also collected and used for background correction of the data. As discussed previously,[49–51] the degree of nanotubes alignment could be directly deduced from the fit of the angular distribution of the scattered intensity at a given wave vector. These distributions were well described by Gaussian functions. The half-width at half maximum of the Gaussian functions was taken throughout this study as the average orientation of the nanotubes or polymer chains along the fiber axis.[52] The wave vector of the diffraction peak, which corresponded to the intertube spacing at 1.85 Å^{-1}, was the one used to characterize nanotube orientation.[53]

The polymer orientation was characterized by the angular distribution of the intensity of the diffraction peak at 1.49 Å^{-1}, which corresponded to the (200) plane of the γ-crystalline form of PA12.[53,54]

Mechanical testing

The mechanical properties of the fibers were characterized under tensile load with a Zwick Roell testing machine equipped with a 10-N load cell. Tests were run on single fibers under a crosshead speed of 1% strain/min with a fiber gauge length of about 25 mm. Before testing, the fibers were mounted on paper frames with cyanoacrylate and a high-strength epoxy adhesives. The fibers were held by screw grips (Zwick Ref 8153) able to withstand a load of 20 N. The diameter of the cylindrical fibers was measured in three equally spaced locations along the gauge length of each sample with an optical microscope. This allowed the diameter uniformity to be verified. It was found to vary along the fiber samples within a margin of no more than 10%.

RESULTS

Morphological analysis

The nanotube–PA12 composite fibers exhibited a uniform texture and diameter, as shown in Figure 2.

The SEM micrographs of the MWNTs before and after melt compounding and washing are shown in Figure 3(a,b), respectively. The nanotube length, initially greater than a few micrometers, clearly decreased after melt compounding down to a few hundreds of nanometers. Nanotubes have to be as long as possible to bring the most effective reinforcement to the composite. Nevertheless, with an average external diameter of about 10–15 nm, even after

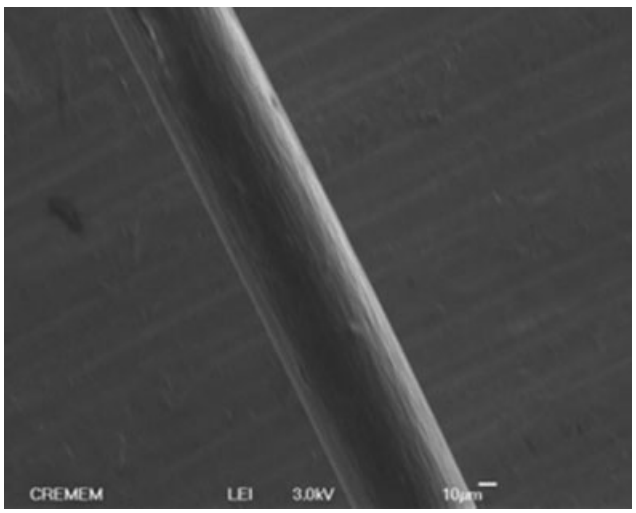

Figure 2 SEM micrograph of a melt-spun PA12–MWNT composite fiber. The nanotube weight fraction of the fiber was 7 wt % (denoted PA12–7NT in the text).

melt compounding, the aspect ratio remained sufficiently large to allow mechanical reinforcements. The nanotubes were also not straight. They exhibited some waviness, which may have, unfortunately, decreased the mechanical reinforcement.[55]

Figure 4 shows SEM images of a PA12–7NT fiber's transversal and longitudinal sections. The well-dispersed bright dots and lines reflect the presence of the nanotubes. The transversal section image [Fig. 4(a)] confirmed the homogeneous dispersion of nanotubes throughout the PA12 matrix. Investigations along the melt-spun fiber axis [Fig. 4(b)] indicated a preferential orientation of the nanotubes along this direction, which is denoted by the arrow.

Fiber linear density (L_d)

We measured L_d by simply weighing samples of given lengths. Knowing the mass fraction P of MWNTs in the composite fibers and the densities of the polymer (ρ_{PA12}) and nanotubes (ρ_{CNT}), respectively, 1.01 g/cm^3 for the PA12 and about 1.8 g/cm^3 for the CNTs, we could deduce the average fiber diameter d from weight m of the fiber sample of length l:

$$d = \sqrt{\frac{4}{\pi l}\left(\frac{Pm}{\rho_{CNT}} + \frac{(1-P)m}{\rho_{PA12}}\right)} = \sqrt{\frac{4L_d}{\pi}\left(\frac{P}{\rho_{CNT} + \frac{(1-P)}{\rho_{PA12}}}\right)} \quad (1)$$

Figures 5 and 6 show the linear density of fibers (unit: 1 tex = 1 mg/m) as a function of the spinning speed for different screw rotation speeds and different nanotube fractions. In both cases, the linear density decreased with spinning speed. L_d is expected to scale as $L_d \approx 1/v$ (where v is the spinning speed) under the assumption of constant volume. The data shown in Figure 5 were in good agreement with this expectation.

The decrease in the screw rotation speed induced a decrease in L_d because of a lower supply rate of composite material. It was in this study of 1 g/min at a screw rotation speed of 10 rpm and of 0.4 g/min at 5 rpm. The ratio of linear densities deduced from the data shown in Figure 5 was 2.8 (930/320, which is the ratio of prefactors of the reciprocal function fits given in the caption of Fig. 5). This was relatively close to the ratio of supply rates, which was 2.5 (1/0.4). However, experiments performed for different fractions of nanotubes and a similar screw rotation speed showed that the nanotube weight fraction did not substantially affect L_d (Fig. 6).

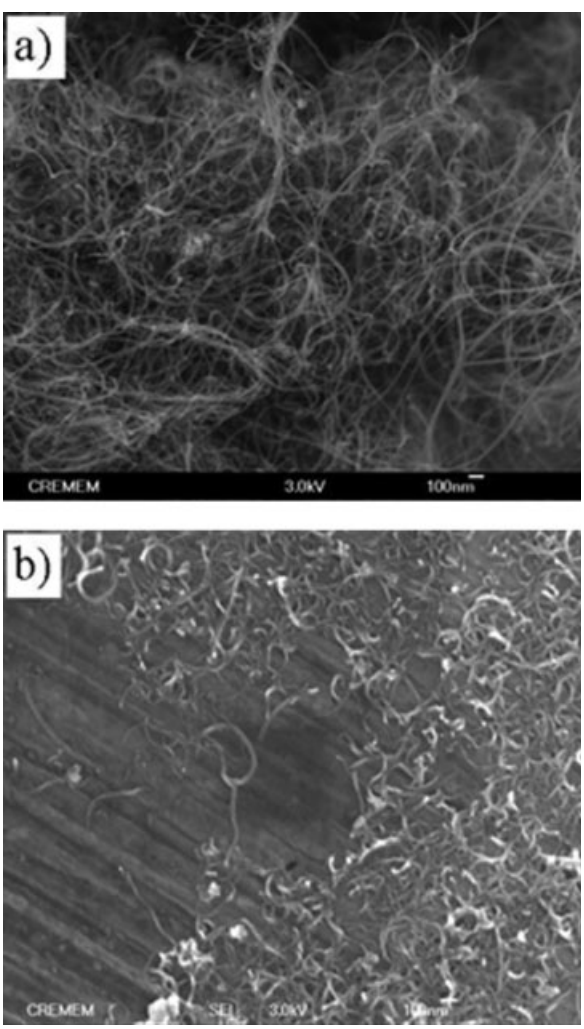

Figure 3 SEM micrographs of MWNTs (a) before and (b) after melt compounding and washing (scale bar = 100 nm).

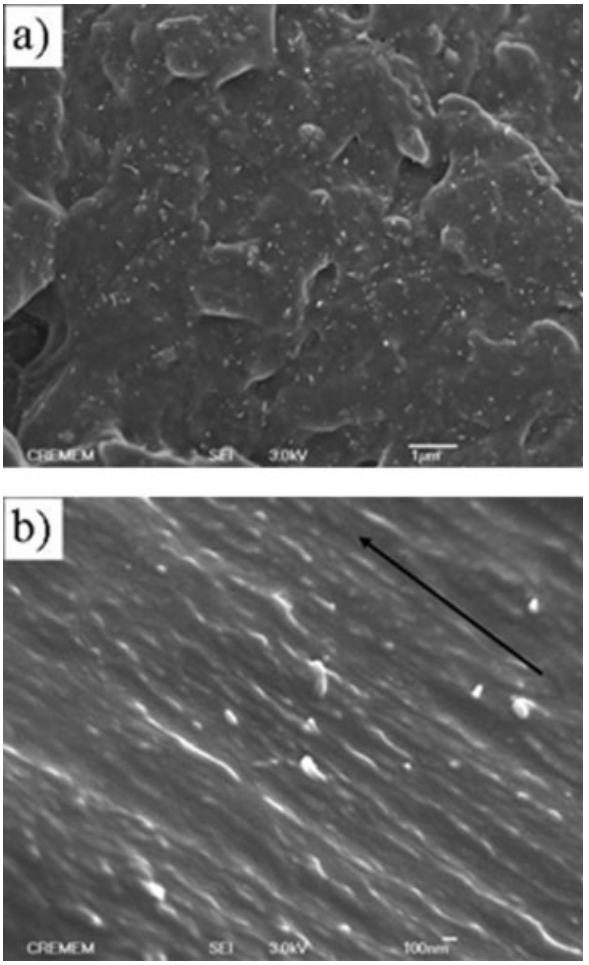

Figure 4 SEM micrographs of (a) a PA12–7NT fiber cross section (scale bar = 1 μm) and (b) a drawn PA12–7NT fiber longitudinal section parallel to the fiber axis (scale bar = 100 nm). The arrow indicates the orientation of the fiber axis.

Influence of the spinning conditions on CNT orientation within the fibers

The effects of the screw rotation speed, spinning speed and draw ratio on CNT and polymer orientation are listed in Table I. For each factor, the other parameters were kept constant for comparison purposes. In this set of experiments, the fibers were drawn directly during spinning with the setup shown in Figure 1. Fibers drawn after spinning by hot stretching in a separate oven are described in the next section.

A decrease in the screw rotation speed barely affected the degree of CNT and polymer alignment. The same observation held for the spinning speed. Indeed, a decrease in the screw rotation speed was equivalent to a decrease in the supply rate of melt composite material. By contrast, an increase in the draw ratio strongly increased both CNT and polymer alignment. On the other hand, postspinning treatment induced mechanical rearrangements, which were more effective at aligning the polymer chains and the CNTs.

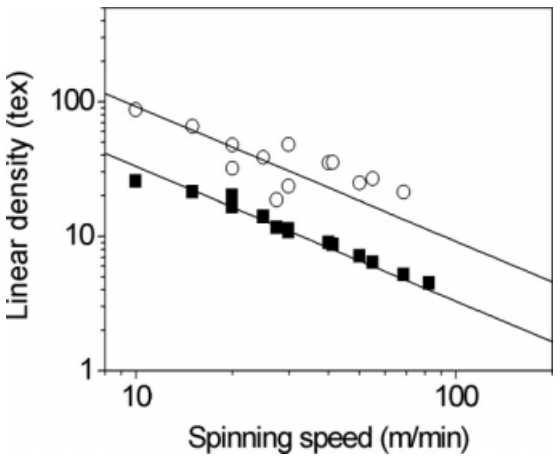

Figure 5 Influence of the spinning speed (v) on the linear density of PA12–nanotube composite fibers. Two different screw speeds were tested: black squares indicate the data obtained with a screw rotation speed of 5 rpm, and white circles indicate the data obtained with a screw rotation speed of 10 rpm. The nanotube weight fraction was 7 wt %. The black lines indicate reciprocal fits: $330/v$ for 5 rpm and $920/v$ for 10 rpm.

Mechanical properties of the fibers

Typical stress–strain curves for neat PA12 and PA12–7NT fibers are shown in Figure 7. We consider in this part fibers that were drawn during spinning (draw ratio = 1–3) and fibers that were drawn after spinning by hot stretching in a separate oven (draw ratio = 5–7). Fibers at these large draw ratios exhibited a greater orientation than the fibers described in the previous section. The alignment of the polymer chains for fibers with a draw ratio of 5 was ±8.5°, and it was ±4.2° for fibers with a draw ratio of 7.

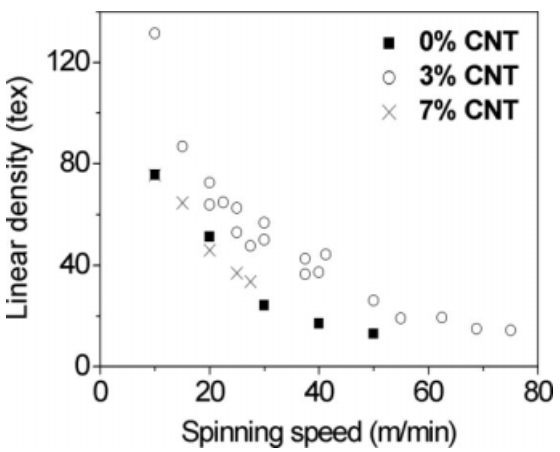

Figure 6 Linear density of the fibers with three different nanotube weight fractions as a function of the spinning speed. The amount of nanotubes did not substantially affect the linear density of the fibers.

TABLE I
Polymer and Nanotube Orientation Along the Fiber Axis for the PA12–7NT Composite Fibers Under Different Spinning Conditions

		Polymer orientation (°)	CNT orientation (°)
Screw rotation speed (rpm)	5	±24.6	±30.1
	10	±31.2	±31.5
Spinning speed (m/min)	10	±34.3	±30.6
	27.5	±31.2	±31.5
Draw ratio	1.5	±33	±37.3
	3	±14.9	±22.7

Three spinning parameters were considered: the screw rotation speed, the spinning speed, and the draw ratio. Each parameter was independently modified. For the screw rotation speed study, the spinning speed and draw ratio were maintained at 27.5 m/min and 1, respectively. For the spinning speed study, the screw rotation speed and drawing ratio were maintained at 10 rpm and 1, respectively. Finally, for the draw ratio study, the screw rotation speed and spinning speed were maintained at 5 rpm and 30 m/min, respectively.

The inclusion of CNTs within the fiber induced a significant increase in the Young's modulus (ca. 75% for the addition of 7 wt % MWNT). However, as shown in Table II, the breaking strength and the elongation at break of the composite fibers were lower.

The results shown in Table II and in Figures 8 and 9 indicate that drawing induced strong modifications of the mechanical properties of both neat and composite fibers. A draw ratio of 7 improved the Young's modulus and the breaking strength of a neat PA12 fiber by about 270% (from 0.9 to 3.3 GPa) and 260% (from 118 to 422 MPa), respectively. In the case of the PA12–7NT fiber, the improvements were slightly lower with about 200% for the Young's modulus (from 1.7 to 5.1 GPa) and 230% for the breaking strength (from 117 to 389 MPa). On the other hand, drawing strongly decreased the elongation at break. It dropped from 337% down to 19% for the neat PA12 fiber and from 146 to 10% for the PA12–7NT fiber.

TABLE II
Effect of the Draw Ratio on the Mechanical Properties of the PA12 and PA12–7NT Fibers

	Draw ratio	Young's modulus (GPa)	Breaking strength (MPa)	Failure strain (%)
PA12	1	0.9	118	337
	3	1.7	228	69
	5[a]	2.4	445	28
	7[a]	3.3	422	19
PA12–7NT	1	1.7	117	146
	2.5	2.7	205	36
	5[a]	4.2	265	9
	7[a]	5.1	389	10

[a] Ratio achieved by hot drawing after spinning.

Figure 10 shows that the majority of the changes in the mechanical properties of the PA12–7NT composite fibers could be ascribed to changes in the polymer orientation. The Young's modulus and breaking strength exhibited similar improvements.

DISCUSSION

To summarize the results, composite fibers made of PA12 and Graphistrength nanotubes were successfully spun down to a diameter of about 50–60 μm for a nanotube weight fraction of about 7 wt %. Fiber drawing allowed the nanotubes and the polymer chains to be aligned. This alignment led to an increase in their elastic modulus, in agreement with

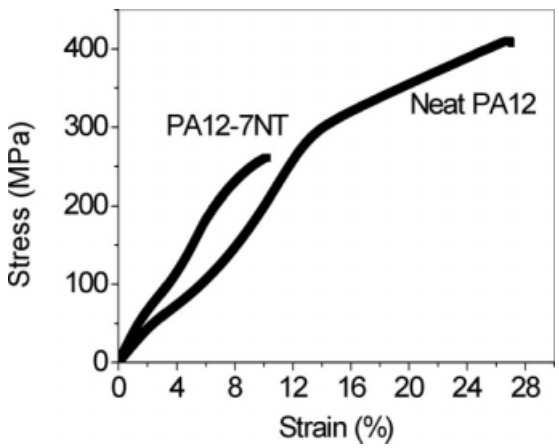

Figure 7 Typical stress–strain curves for a neat PA12 fiber and a nanocomposite PA12–7NT fiber. These fibers were drawn at a ratio of 5, and they both exhibited ±8.5° alignment against the fiber axis. The spinning speeds were 50 m/min for the neat fiber and 137.5 m/min for the composite fiber.

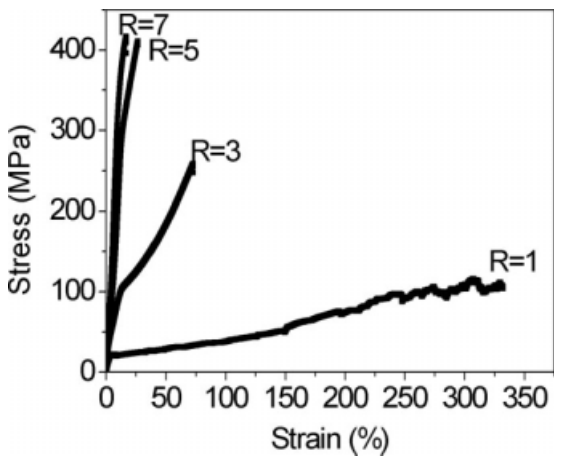

Figure 8 Stress–strain curves of neat PA12 fibers with different draw ratio (R) values. R values of 5 and 7 were achieved after spinning, whereas other R values were directly achieved during spinning.

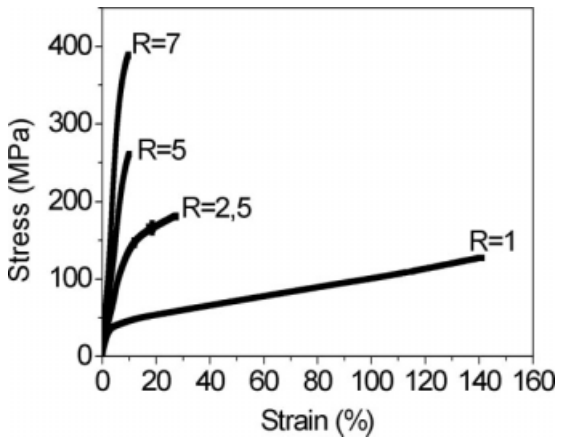

Figure 9 Stress–strain curves of PA12–7NT fibers with different draw ratio (R) values. R values of 5 and 7 were achieved after spinning, whereas other R values were achieved directly during spinning.

previous reports.[36,56,57] The modulus of melt-spun PMMA–SWNT fibers was found to be 6 GPa with 8 wt % nanotubes and an orientation of 4°.[37] This compared well with the properties of our fibers: 5.1 GPa with 7 wt % of CNTs and an orientation of ±4.2°.

For a given level of alignment, we showed that addition of MWNTs led to a further increase in Young's modulus. Such behavior was also consistent with previous reports,[29,35,42,58] even if, in most cases, the orientation of previously investigated systems was not characterized. The increase in the Young's modulus, however, was lower than the modulus, which can be expected from a simple rule of mixture, which assumes a perfect alignment and an efficient stress transfer from the matrix to the nanotubes. It yields

$$E_c = V_f E_f + V_m E_m \quad (2)$$

where E_c, E_f, and E_m are the elastic moduli of the composite fiber, reinforcing fillers, and polymer matrix, respectively, and V_f and V_m the material volume fractions. With $E_f = 500$ GPa and $E_m = 1$ GPa, the modulus expected in this idealized situation would be $E_c = 20.4$ GPa for a fiber that contains 7 wt % nanotubes. We assumed that the density of the nanotubes and PA12 were 1.8 and 1.01 g/cc, respectively. The highest Young's modulus achieved for fibers at 7 wt % nanotubes in this investigation was about 5 GPa. The discrepancy from an optimal reinforcement suggests that the stress transfer and the nanotube alignment were not perfect. The stress transfer can be limited both by the poor adhesion of the nanotubes to the matrix and by the finite length of the nanotubes. More realistic models that take into account limited stress transfer and imperfect alignment have been derived and discussed in the literature.[46–48] They can explain a lower efficiency of composite reinforcements by short fibers. In addition, nanotube waviness can influence the mechanical performance of the composites and yield a lower efficacy of reinforcement.[55]

The failure strain and stress were affected both by the presence of the nanotubes and by the draw ratio. Figure 9 shows that drawing yielded greater strength, but this was associated with a lower failure strain. The nanotubes induced a decrease in the failure strain (Fig. 7), which was consistent with observations made by Siochi et al.[30] for SWNT–polyimide fibers. Sandler et al.[45] also reported a decrease in the elongation at break of PA12 nanocomposite fibers with increasing filler content. Andrews et al.[35] observed a decrease in the tensile strength of MWNT–polystyrene composite films with the addition of nanotubes. They observed similar behavior for the yield strength of MWNT–polypropylene composite fibers. All these previous studies, in addition to this one, suggest that nanotubes act as structural imperfections, which result in premature composite failures. It is, nevertheless, possible that longer nanotubes at higher loadings, with lower waviness, could increase the failure strain and toughness of the fibers. Such enhancements have been observed in other nanotube composite fibers that could absorb a large amount of mechanical energy.[26,59,60]

Investigations of different spinning conditions revealed that the draw ratio was the parameter that led to the most pronounced modifications of the fiber structures and properties. Other factors, such as screw rotation speed and spinning speed, had insignificant effects on the degree of alignment of the nanotubes. However, Shen et al.[39] recently reported an optimal spinning speed to decrease the MWNT waviness and to thereby improve mechanical reinforcement. When spinning is too fast (e.g.,

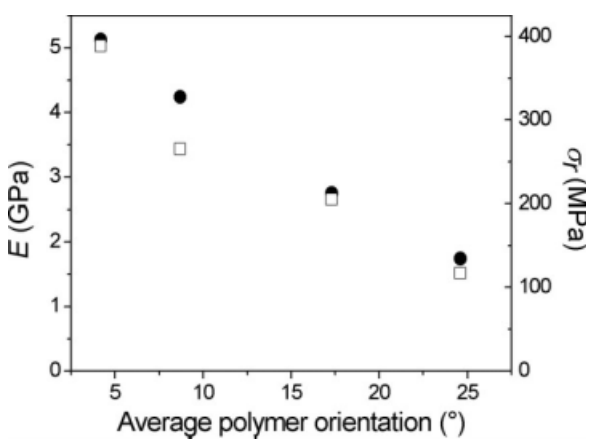

Figure 10 Young's modulus (E) and breaking strength (σ_r) as functions of the polymer chain orientation for a PA12–7NT composite fiber. Black circles correspond to E, and white squares correspond to σ_r.

350 m/min), the MWNTs are unable to respond fast enough, and their waviness remains unaffected. By contrast, when the spinning is too slow (e.g., 150 m/min), the stress experienced by the MWNTs is not strong enough to alter their waviness. Between these two extremes, there may exist an optimal spinning speed where the MWNT waviness can be affected. In our study, the spinning speed was limited to values below 150 m/min. This could explain why no influence of the spinning rate was observed. Nevertheless, varying and increasing the spinning speed remains particularly important for future applications because this parameter will allow the fiber diameters and production rates to be varied.

CONCLUSIONS

The inclusion of CNTs within polymer fibers strongly affected their structure and mechanical properties. Melt-spun PA12–MWNT composite fibers exhibited a greater Young's modulus and breaking strength but a lower failure strain than pure PA12 fibers. This was consistent with the behavior of other nanocomposite fibers investigated previously. Nonetheless, this behavior differed from that of highly loaded composite PVA fibers, which exhibited improvements in their failure strain. Spinning conditions only weakly affected the structure and mechanical properties of melt-spun PA12–MWNT fibers. Nevertheless, the spinning speed remained critical for the production rate of the fibers and for the control of their diameter. Hot stretching, by contrast, induced a substantial improvement in the polymer chain alignment, which was correlated to modifications of the mechanical properties. Future challenges will consist of producing nanocomposite fibers on larger scale with multifilament spinning facilities to test the behavior of these fibers in the form of woven textiles or composites.

The authors thank A. Merceron (Groupement de Recherches de Lacq, Arkema) for technical assistance, Centre de ressources en microcospie électroniqne et microanalyse (CREMEM) for SEM analyses, and B. Kauffmann for his valuable help with X-ray measurements performed at Institut Européen de Chimie et Biologie.

References

1. Wong, E. W.; Sheehan, P. E.; Liebert, C. M. Science 1997, 277, 1971.
2. Yu, M.; Files, B. S.; Arepalli, S.; Ruoff, R. S. Phys Rev Lett 2000, 84, 5552.
3. Yu, M.; Lourie, O.; Dyer, M. J.; Moloni, K.; Kelly, T. F.; Ruoff, R. S. Science 2000, 287, 637.
4. Wagner, H. D.; Lourie, O.; Feldman, Y.; Tenne, R. Appl Phys Lett 1998, 72, 188.
5. Ebbesen, T. W.; Lezec, H. J.; Hiura, H.; Bennett, J. W.; Ghaemi, H. F.; Thio, T. Nature 1996, 382, 54.
6. Hone, J.; Whitney, M.; Piskoti, C.; Zettl, A. Phys Rev B 1999, 59, R2514.
7. Esawi, A. M. K.; Farag, M. M. Mater Des 2007, 28, 2394.
8. Ajayan, P. M.; Tour, J. M. Nature 2007, 447, 1066.
9. Lau, K.; Hui, D. Compos B 2002, 33, 263.
10. Breuer, O.; Sundararaj, U. Polym Compos 2004, 25, 630.
11. Moniruzzaman, M.; Winey, K. I. Macromolecules 2006, 39, 5194.
12. Miyagawa, H.; Misra, M.; Mohanty, A. K. J Nanosci Nanotechnol 2005, 5, 1593.
13. Coleman, J. N.; Khan, U.; Blau, W. J.; Gun'ko, Y. K. Carbon 2006, 44, 1624.
14. Bauhofer, W.; Kovacs, J. Z. Compos Sci Technol 2008.
15. Li, C.; Thostenson, E. T.; Chou, T. Compos Sci Technol 2008, 68, 1227.
16. Fourné, F. Handbook for Plant Engineering, Machine Design and Operation; Hanser: Munich, 1999.
17. Behabtu, N.; Green, M. J.; Pasquali, M. Nano Today 2008, 3, 24.
18. Li, Y.; Kinloch, I. A.; Windle, A. H. Science 2004, 304, 276.
19. Motta, M.; Kinloch, I.; Moisala, A.; Premnath, V.; Pick, M.; Windle, A. Phys E 2007, 37, 40.
20. Zhang, S.; Zhu, L.; Minus, M. L.; Char, H. G.; Jagannathan, S.; Wong, C.-P.; Kowalik, J.; Roberson, L. B.; Kumar, S. J Mater Sci 2008, 43, 4356.
21. Zhang, M.; Atkinson, K. R.; Baughman, R. H. Science 2004, 306, 1358.
22. Jiang, K.; Li, Q.; Fan, S. Nature 2002, 419, 801.
23. Koziol, K.; Vilatela, J.; Moisala, A.; Motta, M.; Cunniff, P.; Sennett, M.; Windle, A. Science 2007, 318, 1892.
24. Vigolo, B.; Pénicaud, A.; Coulon, C.; Sauder, C.; Pailler, R.; Journet, C.; Bernier, P.; Poulin, P. Science 2000, 290, 1331.
25. Ericson, L. M.; Fan, H.; Peng, H.; Davis, V. A.; Zhou, W.; Sulpizio, J.; Wang, Y.; Booker, R.; et al. Science 2004, 305, 1447.
26. Dalton, A. B.; Collins, S.; Munoz, E.; Razal, J. M.; Ebron, V. H.; Ferraris, J. P.; Coleman, J. N.; Kim, B. G.; Baughman, R. H. Nature 2003, 423, 703.
27. Dalton, A. B.; Collins, S.; Razal, J.; Munoz, E.; Ebron, V. H.; Kim, B. G.; Coleman, J. N.; Ferraris, J. P.; Baughman, R. H. J Mater Chem 2004, 14, 1.
28. Zhang, S.; Koziol, K. K. K.; Kinloch, I. A.; Windle, A. K. Small 2008, 4, 1217.
29. Jose, M. V.; Dean, D.; Tyner, J.; Price, G.; Nyairo, E. J Appl Polym Sci 2007, 103, 3844.
30. Siochi, E. J.; Working, D. C.; Park, C.; Lillehei, P. T.; Rouse, J. H.; Topping, C. C.; Bhattacharyya, A. R.; Kumar, S. Compos B 2004, 35, 439.
31. Fischer, D.; Pötschke, P.; Brünig, H.; Janke, A. Macromol Symp 2005, 230, 167.
32. Sennett, M.; Welsh, E.; Wright, J. B.; Li, W. Z.; Wen, J. G.; Ren, Z. F. Appl Phys A 2003, 76, 111.
33. Bhattacharyya, A. R.; Sreekumar, T. V.; Liu, T.; Kumar, S.; Ericson, L. M.; Hauge, R. H.; Smalley, R. E. Polymer 2003, 44, 2373.
34. Dondero, W. E.; Gorga, R. E. J Polym Sci Part B: Polym Phys 2006, 44, 864.
35. Andrews, R.; Jacques, D.; Minot, M.; Rantell, T. Macromol Mater Eng 2002, 287, 395.
36. Haggenmueller, R.; Zhou, W.; Fisher, J. E.; Winey, K. I. J Nanosci Nanotechnol 2003, 3, 105.
37. Haggenmueller, R.; Gommans, H. H.; Rinzler, A. G.; Fisher, J. E.; Winey, K. I. Chem Phys Lett 2000, 330, 219.
38. Moore, E. M.; Ortiz, D. L.; Marla, V. T.; Shambaugh, R. L.; Grady, B. P. J Appl Polym Sci 2004, 93, 2926.
39. Shen, L.; Gao, X.; Tong, Y.; Yeh, A.; Li, R.; Wu, D. J Appl Polym Sci 2008, 108, 2865.
40. Chang, T. E.; Jensen, L. R.; Kisliuk, A.; Pipes, R. B.; Pyrz, R.; Sokolov, A. P. Polymer 2005, 46, 439.

41. Kearns, J. C.; Shambaugh, R. L. J Appl Polym Sci 2002, 86, 2079.
42. Pötschke, P.; Brünig, H.; Janke, A.; Fisher, D.; Jehnichen, D. Polymer 2005, 46, 10355.
43. Schimanski, T.; Peijs, T.; Lemstra, P. J.; Loos, J. Macromolecules 2004, 37, 1810.
44. Hu, X.; Alcock, B.; Loos, J. Polymer 2006, 47, 2156.
45. Sandler, J. K. W.; Pegel, S.; Cadek, M.; Gojny, F.; Van Es, M.; Lohmar, J.; Blau, W. J.; Schulte, K.; Windle, A. H.; Shaffer, M. S. P. Polymer 2004, 45, 2001.
46. Cox, H. L. Br J Appl Phys 1952, 3, 72.
47. Ci, L.; Suhr, J.; Pushparaj, V.; Zhang, X.; Ajayan, P. M. Nano Lett 2008, 8, 2762.
48. Robinson, I. M.; Robinson, J. M. J Mater Sci 1994, 29, 4663.
49. Badaire, S.; Pichot, V.; Zakri, C.; Poulin, P.; Launois, P.; Vavro, J.; Guthy, C.; Chen, M.; Fischer, J. J Appl Phys 2004, 96, 7509.
50. Launois, P.; Marucci, A.; Vigolo, B.; Bernier, P.; Derré A.; Poulin, P. J Nanosci Nanotechnol 2001, 1, 125.
51. Vigolo, B.; Lucas, M.; Launois, P.; Bernier, P.; Poulin, P. Appl Phys Lett 2002, 81, 1210.
52. Pichot, V.; Badaire, S.; Albouy, P. A.; Zakri, C.; Poulin, P.; Launois, P. Phys Rev B 2006, 74, 8.
53. Miaudet, P.; Bartholome, C.; Derré A.; Maugey, M.; Sigaud, G.; Zakri, C.; Poulin, P. Polymer 2007, 48, 4068.
54. Dencheva, N.; Nunes, T. G.; Oliveira, M. J.; Denchev, Z. J Polym Sci Part B: Polym Phys 2005, 43, 3720.
55. Fisher, F. T.; Bradshaw, R. D.; Brinson, L. C. Appl Phys Lett 2002, 80, 4647.
56. Haggenmueller, R.; Du, F.; Fisher, J. R.; Winey, K. I. Polymer 2006, 47, 2381.
57. Thostenson, E. T.; Chou, T. J Phys D: Appl Phys 2002, 35, L77.
58. Fornes, T. D.; Baur, J. W.; Sabba, Y.; Thomas, E. L. Polymer 2006, 47, 1704.
59. Miaudet, P.; Badaire, S.; Maugey, M.; Derre, A.; Pichot, V.; Launois, P.; Poulin, P.; Zakri, C. Nano Lett 2005, 5, 2212.
60. Miaudet, P.; Derre, A.; Maugey, M.; Zakri, C.; Piccione, P. M.; Inoubli, R.; Poulin, P. Science 2007, 318, 1294.